Analyst

Cite this: *Analyst*, 2011, **136**, 3635

www.rsc.org/analyst

PAPER

Real-time electrochemical monitoring of isothermal helicase-dependent amplification of nucleic acids†

Francine Kivlehan,[a] François Mavré,[a] Luc Talini,[b] Benoît Limoges*[a] and Damien Marchal*[a]

Received 8th April 2011, Accepted 24th June 2011
DOI: 10.1039/c1an15289k

We described an electrochemical method to monitor in real-time the isothermal helicase-dependent amplification of nucleic acids. The principle of detection is simple and well-adapted to the development of portable, easy-to-use and inexpensive nucleic acids detection technologies. It consists of monitoring a decrease in the electrochemical current response of a reporter DNA intercalating redox probe during the isothermal DNA amplification. The method offers the possibility to quantitatively analyze target nucleic acids in less than one hour at a single constant temperature, and to perform at the end of the isothermal amplification a DNA melt curve analysis for differentiating between specific and non-specific amplifications. To illustrate the potentialities of this approach for the development of a simple, robust and low-cost instrument with high throughput capability, the method was validated with an electrochemical system capable of monitoring up to 48 real-time isothermal HDA reactions simultaneously in a disposable microplate consisting of 48-electrochemical microwells. Results obtained with this approach are comparable to that obtained with a well-established but more sophisticated and expensive fluorescence-based method. This makes for a promising alternative detection method not only for real-time isothermal helicase-dependent amplification of nucleic acid, but also for other isothermal DNA amplification strategies.

1. Introduction

The development of portable, easy-to-use and inexpensive nucleic acid detection technologies, specially designed for point-of-care diagnosis of infectious diseases at resource-limited locations (*e.g.*, local clinics, small hospitals or in places where the infection originates) would be an important step forward in worldwide public health.[1] However, many nucleic acid assays require sophisticated and costly analytical instruments that cannot be easily operated outside a laboratory environment. This is typically the case for real-time fluorescence-based polymerase chain reaction (PCR) which, regardless of its exquisite sensitivity (single molecule), extreme specific, high accuracy, and ability to provide quantitative results with limited risks of false positive results by cross-contamination, requires relatively bulky, costly, and energy-intensive thermocycling equipments, as well as complex and delicate detection optics that have to be periodically maintained. Consequently, efforts have been made to design simpler miniaturized PCR thermocycling (*e.g.*, using discrete heating zones along a continuous flow-through microfluidic PCR device[2,3] or exploiting a natural convective thermocycler[4]), or to develop isothermal approaches to DNA amplification that do not require temperature-regulating equipment.[5–20] The latter strategy is particularly promising since it offers the possibility of reducing or eliminating the requirement for accurate temperature control and thermocycling, and thus to develop low-cost portable healthcare devices. In the recent years, several isothermal DNA amplification techniques have been proposed as alternatives to PCR, some reaching sensitivities and detection limits similar or equivalent to PCR. The most common isothermal methods include multiple displacement amplification (MDA),[5] nucleic acid sequence-based amplification (NASBA)[6,7] rolling circle amplification (RCA)[8,9] ramification amplification (RAM),[10] helicase-dependent amplification (HDA),[11–15] and loop-mediated isothermal amplification (LAMP),[16–18] each having its own advantages and limitations. The LAMP technique in particular is highly sensitive, rapid and specific, with a detection limit reported as low as a few target DNA copies per assay.[19] It does however involve a complicated amplification reaction scheme that requires the design of multiple primers, which can prove difficult for first-time users. In spite of this, LAMP has been shown in some cases to be faster and more sensitive than PCR, and its integration into a miniaturized microfluidic chip

[a]*Laboratoire d'Electrochimie Moléculaire, UMR 7591 CNRS, Univ Paris Diderot, Sorbonne Paris Cité, 15 rue Jean-Antoine de Baïf, F-75205 Paris Cedex 13, France. E-mail: marchal@univ-paris-diderot.fr; Fax: +33 157278788; Tel: +33 157278898; limoges@univ-paris-diderot.fr; +33 157278788; +33 157278789*
[b]*Easy Life Science, 68, Boulevard de Port-Royal, 75005 Paris Cedex 05, France*

† Electronic supplementary information (ESI) available: Supplementary data associated to real-time fluorescence-based PCR of the plasmid 89-bp target sequence. See DOI: 10.1039/c1an15289k

format coupled to real-time turbid absorbance detection has opened the door to the development of real-time nucleic acid amplification for point-of-use and field analysis.[20,21] Among the other methods, HDA by comparison is a true and much simpler isothermal DNA amplification that employs essentially the same reaction scheme as PCR (*i.e.*, DNA denaturation, primer annealing, and primer extension, including the use of only one primer set), except that the separation of the two complementary DNA strands (or RNA) is achieved enzymatically by employing a thermostable DNA helicase instead of heat used in PCR. Thus, the entire reaction can occur at a single uniform temperature. A detection limit ranging from 10 to 10^3 DNA copies in less than one hour has been reported in many cases.[11,12,22,23] According to its simplicity and isothermal feature, HDA has the potential to be utilized in conjunction with a low-cost portable real-time analyzer capable of performing both the amplification and detection of HDA within the same platform.[24–26]

Another key point for the development of low-cost handheld nucleic acid detection systems is the interfacing of the amplification method with a read-out technology that ideally has to be highly sensitive, cheap, robust, easy to miniaturize, eventually insensitive to colored or cloudy biological samples, and able to operate in real time during the amplification process.[1] While fluorescence-based optical detection methods are well established for monitoring amplified DNA products during a PCR or isothermal DNA amplification (*e.g.*, by monitoring the enhancement of fluorescence of a reporter probe such as a fluorescent dye or a sequence-specific fluorescent oligonucleotide probe that bind to the amplified DNA product), they are not so easy to miniaturize and integrate into low-cost portable devices (*e.g.*, the integration of a laser diode, photodiode, and filter onto a monolithic chip needs sophisticated and costly fabrication processes[3,27]), and moreover they cannot be performed on colored, autofluorescent or cloudy samples. By comparison, electrochemical detection methods can overcome such limitations since they are inherently more robust, simpler, less expensive and easy to miniaturize than optical methods,[28–30] with the further advantages of being able to work in cloudy or even opaque solutions.[31] They are also attractive for the development of handheld diagnostic devices because they require minimal instrumentation, low electrical power supply and no particular need for maintenance or calibration. Although some efforts have been made to combine the advantages of an electrochemical detection with that of a DNA amplification method,[32–35] there is no example where an electrochemical method was used to monitor in real-time an isothermal DNA amplification.

In this paper, we report for the first time the utilization of an electrochemical detection method for monitoring in real-time the isothermal HDA of a DNA target sequence. The detection strategy is similar to that recently developed by us for real-time electrochemical-based PCR.[35] It uses a DNA intercalating redox probe, which upon binding to the amplified double-stranded DNA (ds-DNA) becomes less electrochemically detectable compared with its free counterpart. The principle is therefore analogous to that of real-time HDA assays that employ fluorescent DNA intercalating dyes,[25] except that the measured electrochemical signal follows an exponential decrease with time as the amount of amplified DNA target increases (Fig. 1). The selected redox probe, the $Os[(bpy)_2DPPZ]^{2+}$ (with bpy = 2,2′-bipyridine and DPPZ = dipyrido[3,2-*a*:2′,3′-*c*]phenazine), is the same as previously reported.[35] This is a one-electron reversible redox probe that strongly and specifically binds to ds-DNA and that is sensitively detected by square-wave voltammetry (SWV) down to nanomolar concentrations.[35] To demonstrate the principle of the method and its great potential in the fabrication of a low-cost and simple portable device, we also report on the development of an electrochemical instrument able to automatically monitor in parallel and in real-time up to 48 isothermal HDA reactions in a disposable microplate of 48-electrochemical microwells.

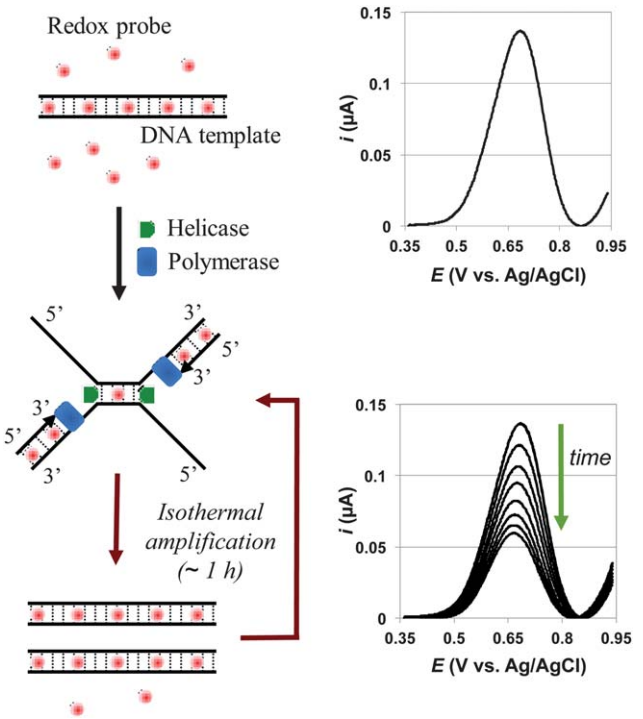

Fig. 1 (Left) Scheme's principle of the real-time electrochemical-based HDA. It relies on the use of two primers and two enzymes (DNA helicase and polymerase). The helicase enzymatically unwinds the DNA template to generate single-stranded DNA for primer hybridization and subsequent extension by the polymerase. As the amount of ds-DNA exponentially grows with time in solution, the amount of free intercalating redox probe decreases at the expense of binding with ds-DNA, and consequently (right) the SWV current response of the redox probe is decreased.

The proof-of-principle of real-time electrochemical-based HDA is demonstrated for the amplification of an 89-base pair (bp) DNA sequence from *E. coli* plasmid, that serves here just as a model target. The analytical performances of the real-time electrochemical-based HDA were evaluated and compared with those of real-time fluorescence-based HDA, which uses EvaGreen® as an intercalating fluorescent dye. We also report the possibility to perform a DNA melt curve analysis at the end of the isothermal amplification, and therefore differentiate specific from non-specific amplifications.

2. Experimental

2.1. Materials and reagents

All reagents were purchased commercially and are of analytical grade, unless otherwise stated. IsoAmp® II Universal tHDA kit

was used for HDA experiments (New England Biolabs Inc.). LITMUS 28i, a plasmid vector from *E. Coli* ER2738, was purchased from New England Biolabs Inc. Reagents used in PCR reactions: 10× PCR buffer, 25 mM $MgCl_2$, 10 mM dNTPs, and 250 U HotStarTaq polymerase were purchased from QIAGEN and were of PCR grade. Primers were designed using Primer Express 3.0 (Applied Biosystems) and prepared as 100 μM stock solutions. The set of primers used in the amplification of the LITMUS 89-bp amplicon (New England Biolabs Inc.) are for the forward primer TAGGGTTGAGTGTTGTTC CAGTTTG (25-bp, T_m = 60 °C) and for the reverse primer CTGATAGACGGTTTTTCGCCCTTT (24-bp, T_m = 62 °C). This set of primers are responsible for the amplification of an 89-bp target of position 1223–1311 of the LITMUS 28i vector sequence, with a calculated melting temperature (T_m) of 78 °C.

Water used in all experiments was of molecular biology grade, and DNase, RNase and Protease free (5′ PRIME). EvaGreen® was used as the fluorescent dye in real time PCR and real time HDA experiments (20×, Biotium), with ROX employed as a reference dye (50×, Invitrogen). Bovine serum albumin (BSA) was purchased from Sigma–Aldrich, with solutions prepared as a 2% (w/v) stock for use in experiments. The osmium redox compound, $Os[(bpy)_2DPPZ](PF_6)_2$, was synthesized in accordance with protocols previously established.[36] HDA or PCR products were also analyzed by gel electrophoresis using E-Gel® pre-cast HR agarose gels (4% agarose with EtBr, Invitrogen) and a 25-bp DNA ladder (Invitrogen).

2.2. Setups of real-time DNA amplification methods

Real-time fluorescence-based HDA and PCR were both monitored using EvaGreen® as the fluorescent intercalating dye, in conjunction with an ABI 7500 real-time PCR machine (Applied Biosystem Instruments).

For real-time electrochemical-based HDA, experiments were carried out using a custom designed single-use 48-well electrochemical microplates, whereby the flat bottom of each well was integrated with 3 screen-printed electrodes: a carbon working electrode (area of 4.8 mm^2), a carbon counter electrode, and a silver pseudo-reference (LEO, Easy Life Science, www.elice.fr). Once each well was sealed closed with a standard cap normally used to close PCR microtubes (*i.e.*, caps used for PCR microtubes), it forms a self-contained electrochemical cell (working volume ranging from 25 to 75 μL) that can be individually used electrochemically. The 48-well electrochemical microplates were used in conjunction with a modified thermocycler consisting of a flat Peltier heat block equipped with two protruding arrays of 72-pin connectors and a PCB interface for the 48-channel multipotentiostat (Easy Life Science). With such equipment, the overall 48-electrochemical wells can be scanned quasi-simultaneously by SWV from 0.35 V to 0.95 V (*vs.* Ag/AgCl) in less than 3 seconds (multiplexed acquisition with the following SWV parameters: frequency of f = 100 Hz, pulse amplitude of ΔE_p = 40 mV, and potential step increment of E_{SW} = 5 mV). During the experiment, the faradic square wave peak current responses, I_p, of the overall square wave voltammograms were automatically extracted using a home-made program (using MATLAB software), resulting finally in a plot of I_p as a function of amplification time.

HDA reactions were performed in accordance with standard protocols described for the IsoAmp® II kit. This consisted of a 50 μL volumes, combining the various components: 1× annealing buffer II, 4 mM $MgSO_4$, 40 mM NaCl, 7% v/v dNTPs/enzyme mixes, 0.025% BSA, 75 nM or 175 nM primers and different concentrations of the LITMUS 28i vector template. For experiments based on fluorescence detection, 0.2× EvaGreen® and 1× ROX were included, while those based on electrochemical detection required 0.5 μM $Os[(bpy)_2DPPZ]^{2+}$. All preparations of mixes were done on ice. Real-time monitoring of DNA amplification was performed at 65 °C by recording fluorescence every 2 min during 120 min on the ABI 7500 instrument or by recording SWV current response every 38 s during 80 min on the LEO instrument. Melt curve analysis was performed immediately following amplification, starting with a denaturation step at 95 °C for 1 minute, followed by a cooling step at 40 °C for 1 minute, and then continuous melt curve data acquisition every 20 seconds during a 1.3 °C min^{-1} ramp to 90 °C for the ABI 7500 instrument, or every 13 seconds during a 1 °C min^{-1} ramp to 90 °C for the LEO instrument.

PCR reactions were prepared as 50 μL volumes, combining the various components: 1× QIAGEN PCR Buffer, 0.1 mM dNTPs, 1.25 Units HotStarTaq, 1.75 mM $MgCl_2$, 75 nM primers, 1× EvaGreen®, 1× ROX and different concentrations of LITMUS 28i vector template. The temperature cycle program consisted of an initial denaturation step at 95 °C for 15 minutes, followed by 40 cycles (consisting of 95 °C for 50 seconds, 58 °C for 1 minute and 72 °C for 30 seconds), and then a final extension step at 72 °C for 1 minute.

3. Results and discussion

3.1. Development of a disposable electrochemical microplate of 48 microwells and subsequent connection to a multipotentiostat and heat block

With the aim to demonstrate the possibility to have a low-cost device that can electrochemically monitor automatically and in parallel multiple isothermal HDA reactions, we have developed a disposable electrochemical microplate of 48 independent microwells, with three screen-printed electrodes (Fig. 2A). Each well can be filled with a working volume ranging from 25 to 75 μL (in the present work, we have used 50 μL), and sealed closed with a standard cap to avoid evaporation during the isothermal amplification. The microplate was fabricated by bonding of a square molded plastic plate (10 × 10 cm) consisting of 48 cylindrical holes (0.6 cm diameter) and a flat support on which 48 × 3 electrode arrays were screen-printed. The fabrication process is easy to implement within an industrial process, for the mass-production of low-cost disposable electrochemical microplates. For heating we have used a standard thermocycler where the classical Peltier heat block for microtubes was replaced by a flat heat block laterally incorporating two arrays of 72-pin connectors on the surface. For connection with a multipotentiostat, the connectors on the block were connected to a PCB interface placed just behind the thermocycler (Fig. 2B). The PCB interface has been specifically designed for monitoring quasi-simultaneously the 48 microwells by SWV according to a multiplexed 48-channel electronic scheme. For an experiment,

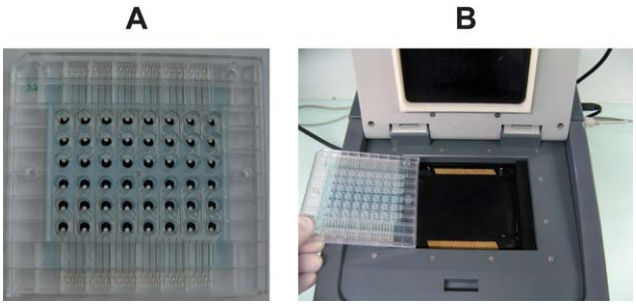

Fig. 2 (A) Disposable electrochemical microplate of 48 independent microwells, each equipped on their flat bottom with 3 screen-printed electrodes. (B) Standard thermocycler equipped with a flat heat block incorporating two arrays of 72-pin connectors, ready to receive a disposable electrochemical microplate of 48 independent microwells. The microplate is connected to a multiplexed potentiostat PCB interface placed just behind the thermocycler (not visible in the image).

an electrochemical microplate is placed on the flat heat block and then simply electrically connected to the underlying arrays of 72-pin connectors by closing the unit cover. With this configuration, the overall electrochemical microwells can be heated at a uniform constant temperature of 65 °C and at the same time scanned by SWV throughout the isothermal HDA. The SWV technique was selected because of its high sensitivity compared with other electroanalytical methods, its rather fast acquisition time, and the ease to extract the analytical information from the Gaussian-shaped peak that is typically obtained for redox compounds able to rapidly and reversibly exchange their electrons. Under the selected conditions, it was possible to monitor the overall 48 electrochemical wells in less than 3 seconds.

3.2. Design of a real-time fluorescence-based HDA for quantitative detection of an 89-bp target sequence of *E. coli* plasmid

Because HDA is not successful with DNA fragments longer than 100-bp, we have chosen to design a HDA reaction for an 89-bp target sequence from *E. coli* plasmid (vector LITMUS 28i). Prior to considering electrochemical detection, we determined the conditions suitable to quantitatively detect this target in real-time fluorescence-based HDA, using EvaGreen® as a fluorescent intercalating dye. Fig. 3 shows the amplification curves generated at a constant temperature of 65 °C from serial dilutions (10-fold) of DNA template and using an IsoAmp® II Universal kit. In agreement with the enhancement of EvaGreen® fluorescence upon its intercalation into the amplified ds-DNA product, the real-time amplification curves show a characteristic exponential increase of fluorescence as a function of amplification time (Fig. 3A). The onset of fluorescence increase depends linearly on the logarithm of the starting number of DNA template copies. The point at which the signal increase crosses a fixed threshold time value (dashed horizontal line in Fig. 3B), results in a semi-logarithmic calibration plot shown in Fig. 3C.

From the semi-logarithmic calibration plot (Fig. 3C), a linear working concentration range between 10^5 and 5×10^9 initial target copies per assay was determined, with a detection limit of $\sim 10^5$ initial target copies. From the slope of the linear regression, an amplification efficiency of 1.6 was calculated. This latter value indicates that the target DNA concentration in the reaction solution is doubled every 90 s. The detection limit is not as good as that usually obtained with HDA.[11,12,22,23] It is limited by an early nonspecific fluorescence increase of the negative template control (NTC). This problem was identified as being related to the nonspecific amplification of primer–dimers, leading thus to a nonspecific binding of EvaGreen®. This was confirmed by the presence of a low molecular weight band on the post-amplification electrophoretic gel for the NTC and also by the observation of a low melting temperature peak in the melt curve of some positive controls and the NTC (*vide infra*). With the aim to compare these results with a more conventional and widely used real-time amplification technique, the calibration plot of the 89-bp plasmid target was established for real-time fluorescence-based PCR using EvaGreen® as the intercalating dye (see, Fig. S1†). A significantly lower nonspecific response was observed in real-time PCR, allowing thus to achieve a 100-fold lower detection limit compared to real-time HDA. The noteworthy nonspecific response in real-time HDA suggests a problem of specificity with the selected primers. To reduce as much as possible the amplification of primer–dimers during the HDA reaction, it would be useful to redesign and/or optimize the primers as well as the overall constituents of the HDA mix.[23]

3.3. Proof-of-concept of the real-time electrochemical-based HDA

Fig. 4 shows typical amplification curves recorded at 65 °C during real-time electrochemical-based HDA for three different reactions: (1) a positive control (5×10^7 DNA target copies), (2) a NTC (no target), and (3) a negative control (in which dNTPs were omitted). Each reaction contained 175 nM primers and 0.5 μM $Os[(bpy_2)DPPZ]^{2+}$.

The raw data are shown in Fig. 4A. At the beginning of the reaction, all three reactions show a continuous and nearly linear increase of the SWV peak current response (I_p) as a function of amplification time (see Fig. 1 for an illustrating example of experimental SWV responses). We have attributed this positive drift to a favorable partitioning (or adsorption) of the $Os[(bpy_2)DPPZ]^{2+}$ redox probe to the surface of the working carbon electrode. This statement is supported by the fact that a significant enhancement of the slope of current increase as a function of time was obtained when BSA or unrelated nucleic acids were deliberately added to the solution. These results are in line with the formation of a thin anionic film of these negatively charged macromolecules on the electrode surface, which therefore leads to an accumulation of the positively charged redox probe on the working electrode and thus an enhancement of the current response. It is worth noting that BSA was systematically added to the reaction solution in order to prevent possible inhibition of HDA by the adsorption of enzymes on the microwell surface. For the true negative control, which thus does not contain dNTPs, the SWV current grows approximately linearly at the beginning of the amplification time and then slightly slowly at longer times (curve 3 in Fig. 4A). The shape of this true blank response can be well-fitted to a quadratic equation. For the positive control, the behavior is in stark contrast to the negative one since after the initial phase of signal increase, we observed

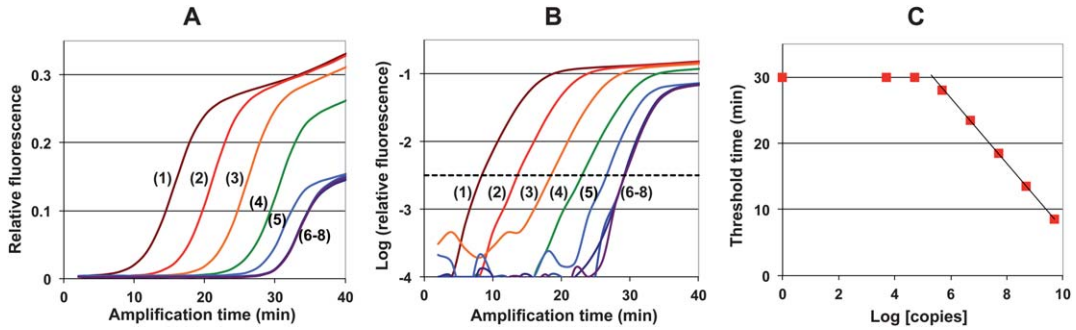

Fig. 3 (A and B) Isothermal amplification curves ($T = 65$ °C) obtained for the real-time fluorescence-based HDA of an 89-bp plasmid DNA sequence. The concentration of primers in each reaction solution was 75 nM and the initial number of target DNA copies per assay was: (1) 5×10^9, (2) 5×10^8, (3) 5×10^7, (4) 5×10^6, (5) 5×10^5, (6) 5×10^4, (7) 5×10^3, and (8) 0 (NTC). (B) Semi-logarithmic representation of plots in (A) after a linear baseline correction (the horizontal dashed line indicates the threshold level used to establish the calibration curve in (C)). (C) Calibration plot of the threshold time as a function of logarithmic input of DNA target copies. The black line is a linear regression fitted to the highest concentrations (slope: −4.9, intercept: 56.5, $r = 0.9995$).

a sudden decrease at a defined amplification time (~30 min) (curve 1 in Fig. 4A). A similar response was also obtained for the NTC, but the onset of current decrease was observed at a later amplification time (~50 min). The signal decrease observed for both samples suggests an effective production of ds-DNA in the electrochemical microwell, which, at a given amplification time, reaches a threshold concentration value sufficient to bind a fraction of intercalating redox probe in solution, leading thus to a detectable signal decrease. The fact that the onset of signal decrease appears sooner for the positive control than for the NTC signifies a specific target amplification in the solution of the positive control. But, in view of the false positive response of NTC, there is also some significant nonspecific ds-DNA amplification. We have attributed this nonspecific amplification to the nonspecific production of primer–dimers, also observed in fluorescently monitored real-time HDA. This was confirmed by the presence of a band of low molecular weight on the post-amplification electrophoretic gel (inset of Fig. 4C), characteristic of primer–dimer formation. For the positive control, a band of higher molecular weight (~90-bp) is obtained, close to that expected for the target.

In order to read amplification curves in a clear manner, the data were systematically corrected from the current drift occurring in the absence of any signal decrease by subtraction of an extrapolated least-square fitted quadratic line across the early amplification time (represented by the dashed lines in Fig. 4A). The corrected amplification curves (Fig. 4B) were finally plotted in a more conventional semi-logarithmic representation (Fig. 4C), similar to that obtained in fluorescence. These results finally clearly demonstrate the feasibility of this proposed method.

3.4. Comparative study between electrochemically and fluorescently monitored real-time HDA

To evaluate and compare the analytical performances of the electrochemical method with that of fluorescence, the calibration plot of the plasmid DNA target has been established in real-time electrochemical-based HDA under similar experimental conditions to those used in fluorescence (*i.e.*, same primers and enzyme concentrations, buffer constituents and temperature processing), except for the intercalating probe which was of course different.

The real-time amplification curves generated from a primer concentration of 75 nM and serial dilutions (10-fold) of the plasmid DNA template are shown in Fig. 5, as well as the resulting calibration plot. Although the amplitudes of current decrease were significantly lower than those previously obtained in Fig. 4, it was possible to extract from the corrected baseline

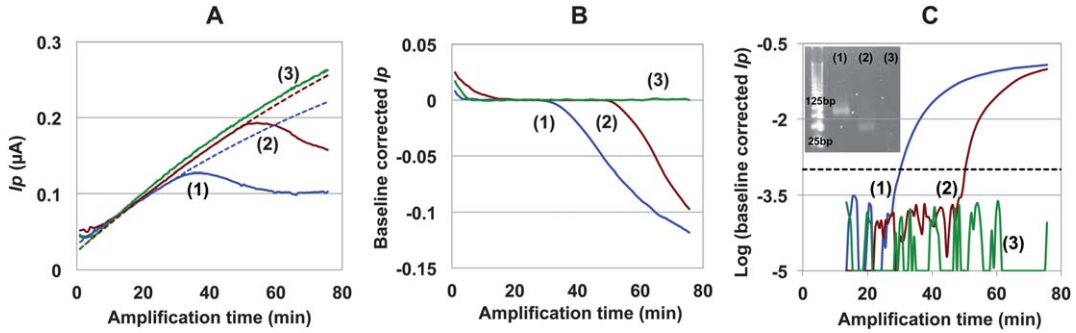

Fig. 4 (A) Isothermal amplification curves ($T = 65$ °C) obtained for the real-time electrochemical-based HDA of an 89-bp plasmid DNA sequence: (1) positive control (5×10^7 copies), (2) NTC, (3) negative control without dNTPs. The primers and $Os[(bpy_2)DPPZ]^{2+}$ concentrations were 175 nM and 0.5 µM, respectively. Solid lines: experimental I_p values *vs.* amplification time. Dashed lines: second-order polynomial fits. (B) Same as in (A) but after baseline correction. (C) Same as in (B) but on a logarithmic scale. Inset: gel electrophoresis image of the post-HDA solutions.

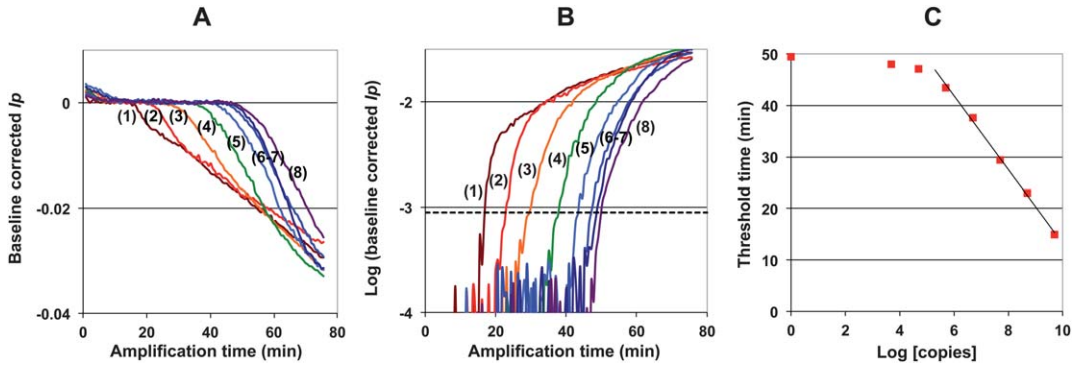

Fig. 5 (A and B) Isothermal amplification curves ($T = 65$ °C) obtained for the real-time electrochemical-based HDA of an 89-bp plasmid DNA sequence. The concentration of primers in each reaction solution was 75 nM and the initial number of target DNA copies per assay was: (1) 5×10^9, (2) 5×10^8, (3) 5×10^7, (4) 5×10^6, (5) 5×10^5, (6) 5×10^4, (7) 5×10^3, and (8) 0 (NTC). (B) Semi-logarithmic representation after linear baseline correction. (C) Calibration plot: the black line is a linear regression fitting to the highest concentrations (slope: −7.2, intercept: 85 min, $r = 0.9975$).

amplification plots (Fig. 5A and B) a threshold amplification time that was linearly proportional to the initial copies of DNA target (Fig. 5C). From the semi-logarithmic calibration plot, a linear working concentration range between 10^5 and 5×10^9 initial target copies per assay was obtained, with a detection limit of $\sim 10^5$ copies. These results are very similar to those obtained in fluorescence. From the slope of the calibration plot, an amplification efficiency of 1.4 could be estimated, which is acceptable but somewhat lower than in real-time fluorescence-based HDA (1.6). Such a value signifies that the target DNA concentration is doubled every ~120 s, instead of every 90 s as with the fluorescence method.

To test the influence of primer concentration on the analytical performances of the electrochemical HDA and more specifically on the signal amplitude and nonspecific response, a second calibration plot was achieved for a higher starting primer concentration of 175 nM. By increasing the primer concentrations, we can thus hope to improve the end-product yield of HDA. The overall results are summarized in Fig. 6. As expected from the increase of DNA product yield, the signal amplitudes observed in the real-time amplification plots were higher, thus making it easier to extract the threshold amplification time. However, by comparison with the data reported at lower primer concentrations, the dynamic range was narrower (10^6 and 5×10^9 copies) and the detection limit 10-fold higher (Fig. 6C). These results could be explained by an earlier nonspecific current decrease at higher primer concentrations, which therefore adversely affects the detection limit. This is consistent with an increase of nonspecific amplification of primer–dimer formation resulting from the use of higher starting primer concentrations.

With the aim to better compare the electrochemical and fluorescent-based HDA methods, the calibration plots of both approaches were repetitively repeated in triplicate under similar experimental conditions and for the same 10-fold serial dilutions of DNA template. The results for both methods are reported on the same graph in Fig. 7.

A comparative study of the two calibration plots shows similar detection limits and reproducibility but dissimilar amplification efficiencies, confirming a faster amplification rate with the fluorescence-based method. A possible reason for such a difference can be a larger inhibition of the isothermal DNA amplification by the osmium intercalating probe than by the EvaGreen® fluorescent dye (EvaGreen® is known to slightly inhibit HDA, but less than other fluorescent dyes[25]). We have indeed found in

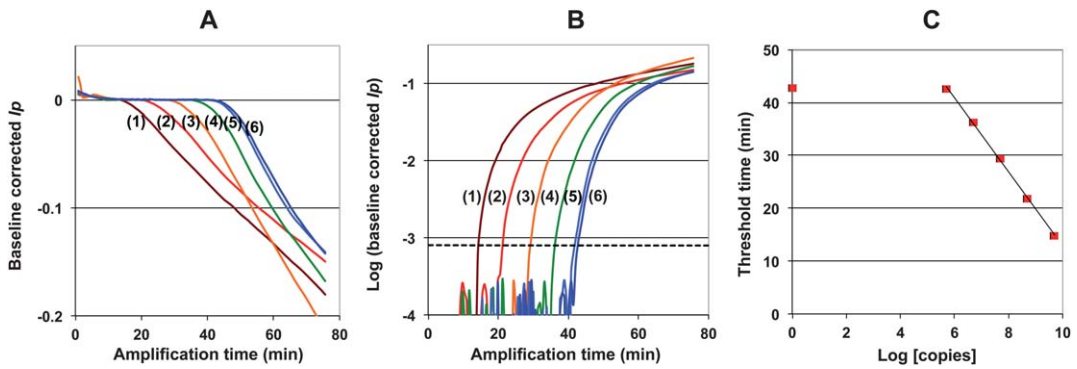

Fig. 6 (A and B) Isothermal amplification curves ($T = 65$ °C) obtained for the real-time electrochemical-based HDA of an 89-bp plasmid DNA sequence. The concentration of primers in each reaction solution was 175 nM and the initial number of target DNA copies per assay was: (1) 5×10^9, (2) 5×10^8, (3) 5×10^7, (4) 5×10^6, (5) 5×10^5, and (6) 0 (NTC). (B) Semi-logarithmic representation of plots in (A) after a linear baseline correction (the horizontal dashed line indicates the threshold level used to establish the calibration curve in (C)). (C) Calibration plot: the black line is a linear regression fitting to the highest concentrations (slope: −7.2, intercept: 85 min, $r = 0.9984$).

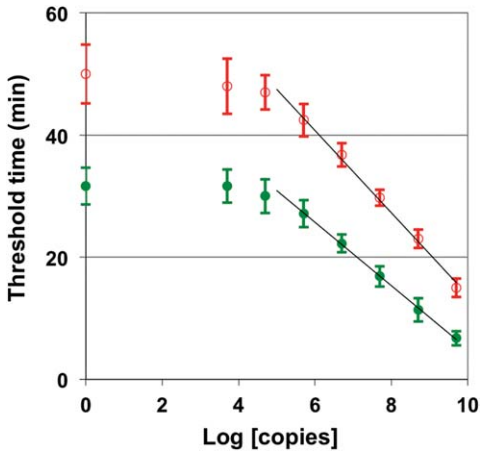

Fig. 7 Standard calibration plots of the 89-bp plasmid DNA target obtained (○) in real-time electrochemical-based HDA and (●) real-time fluorescence-based HDA. Each study was done in triplicate. Error bars represent standard deviation. Straight lines were obtained from linear regression fitting to the highest concentrations: (○) slope: −6.7, intercept: 81 min, $r = 0.9974$; (●) slope: −5.2, intercept: 56.8 min, $r = 0.9995$.

the presence of an increasing concentration of Os[(bpy_2)DPPZ]$^{2+}$ that a growing inhibition of HDA occurs. It is therefore reasonable to suppose that some inhibition should continue to prevail at the Os[(bpy_2)DPPZ]$^{2+}$ concentration of 0.5 μM used during real-time electrochemical-based HDA. A lower redox probe concentration should certainly be helpful to further reduce the inhibition and therefore improve the amplification efficiency, but it has not been tested because the electrochemical response becomes too low to be suitably detected.

Concerning the threshold amplification time reproducibility, it can be roughly estimated from the relative standard deviations of data reported in Fig. 7. An average relative value of ± 8% was calculated for both methods.

3.5. Melt curve analysis

A further interesting aspect of using intercalating probes in real-time HDA is the possibility to discriminate, at the end of amplification, full length amplicons from shorter products (such as primer–dimers) by a melt curve analysis.[25] To achieve this, a linear ramp of temperature (1 °C min^{-1}) was applied to the reaction solutions immediately after the HDA was completed, and a series of SWV measurements were recorded once every 13 s throughout the scanned temperature range (from 60 to 95 °C). As the temperature reaches the melting point of an amplicon, a sharp increase in current response can be observed upon the release of the intercalated redox probe into the bulk of solution.[35]

Fig. 8 shows the melt curves (and their corresponding first derivative) which were recorded at the end of the real-time electrochemical-based HDA experiment previously shown in Fig. 5. Shown also in Fig. 8 are the melt curves recorded at the end of the real-time fluorescence-based HDA experiment presented in Fig. 3. A very good agreement between the electrochemical and fluorescence melt curves was obtained, especially for the first derivative plots which both show for highly positive samples the presence of a high melting temperature peak (T_m = 81 °C for the electrochemical detection and T_m = 80 °C for the

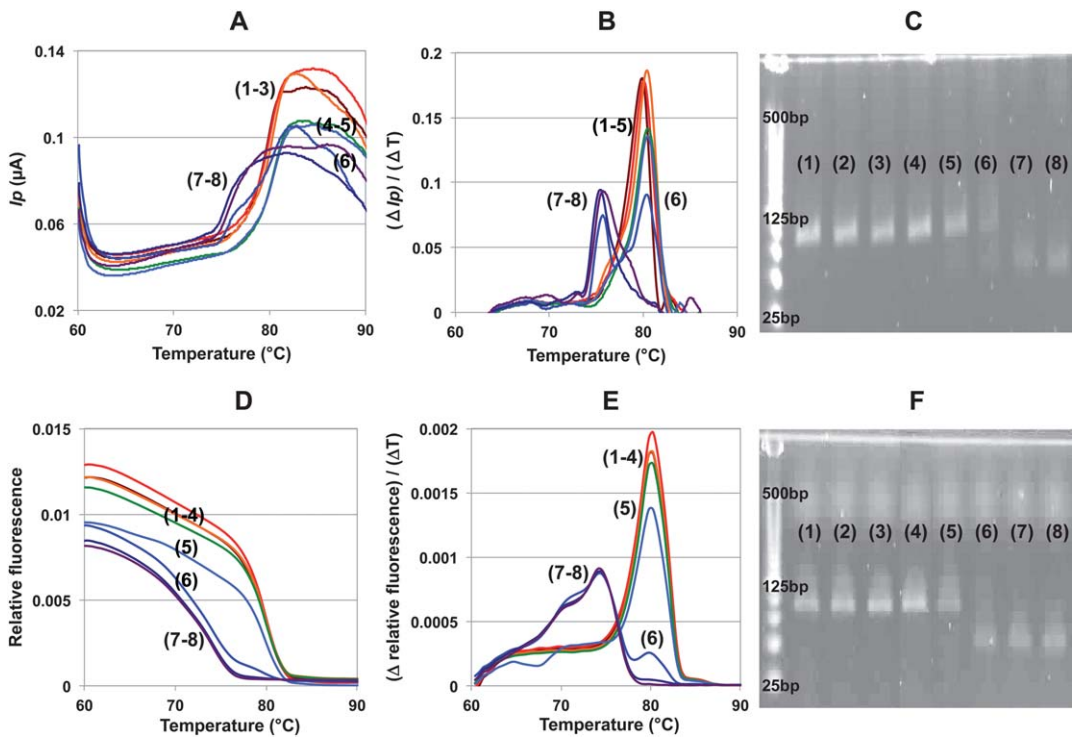

Fig. 8 (A and B) Electrochemical-based and (D and E) fluorescence-based melt curves recorded after the real-time HDA amplification experiments presented in Fig. 5 and 3, respectively. (B and E) First derivative plots. (C and F) Gel electrophoresis images of the end-HDA products resulting from the (C) electrochemical and (F) fluorescence approach. The initial number of target DNA copies per assay are the same as in Fig. 5 and 3, *i.e.*: (1) 5×10^9, (2) 5×10^8, (3) 5×10^7, (4) 5×10^6, (5) 5×10^5, (6) 5×10^4, (7) 5×10^3, and (8) 0 (NTC).

fluorescence detection) that is attributed to the 89-bp amplicon. For the negative control or positive controls containing low initial target DNA copies, another peak was obtained at lower melting temperature ($T_m = 76$ °C for the electrochemical detection and $T_m = 74$ °C for the fluorescence detection), which is characteristic of the presence of primer–dimer formation. These results were confirmed by gel electrophoresis analysis of the post-amplified solutions, which showed qualitatively the same trend. It is interesting to note that melt curve analysis helps to differentiate true positive samples from false negative ones down to a concentration as low as 5×10^4 target copies. The end-point melt curve analysis is therefore a useful complementary tool for isothermal amplification plots, which not only help to discriminate true from false positive samples but also to distinguish lower DNA template concentrations.

4. Conclusions

We have demonstrated, for the first time, the feasibility to monitor electrochemically and in real time an isothermal HDA amplification. The method was demonstrated to be able to quantitatively analyze a target nucleic acid under isothermal conditions in less than one hour and to perform a DNA melt curve analysis at the end of amplification for discrimination between specific and non-specific amplifications. The methodology described here compares well with conventional real-time fluorescence methods which use intercalating fluorescent dyes, thus sharing the same advantages, but with the additional advantages of being potentially more robust, simpler, less expensive and easier to integrate in a handheld device for point-of-care nucleic acid testing. Moreover, on account of the relative insensitivity of electrochemical methods to downscaling, the detection scheme is expected to be particularly useful in miniaturized devices such as in a microchip platform or in a microfluidic system. The method was validated with a thermal system that at present is not transportable, but could be easily replaced by a much lightweight and compact heating system such as a simple thin-film resistance heater with passive or fan-assisted cooling.[37,38] Owing to the quite general applicability of the detection scheme's principle, it should be easily extended to many other isothermal DNA amplification strategies as well as to the achievement of quantitative nucleic acid assays for point-of-care applications such as the screening and surveillance of an epidemic virus (*e.g.*, SARS, tuberculosis, malaria, influenza A) or the diagnosis of multiresistant bacteria (*e.g.*, MRSA), to just cite a few.

Acknowledgements

This research was supported by Université Paris Diderot and CNRS. We acknowledge the Agence Nationale de la Recherche for the financial support and salary of FK, and Easy Life Science for its participation.

References

1 T. M.-H. Lee and I.-M. Hsing, *Anal. Chim. Acta*, 2006, **556**, 26–37.
2 M. U. Kopp, A. J. de Mello and A. Maz, *Science*, 1998, **280**, 1046–1048.
3 Y. Zhang and P. Ozdemir, *Anal. Chim. Acta*, 2009, **638**, 115–125.
4 N. Agrawal, Y. A. Hassan and V. M. Ugaz, *Angew. Chem., Int. Ed.*, 2007, **46**, 4316–4319.
5 F. B. Dean, S. Hosono, L. Fang, X. Wu, A. F. Faruqi, P. Bray-Ward, Z. Sun, Q. Zong, Y. Du, J. Du, M. Driscoll, W. Song, S. F. Kingsmore, M. Egholm and R. S. Lasken, *Proc. Natl. Acad. Sci. U. S. A.*, 2002, **99**, 5261–5266.
6 J. Compton, *Nature*, 1991, **350**, 91–92.
7 T. Kievits, B. Van Gemen, D. Van Strijp, R. Schukkink, M. Dircks, H. Adriaanse, L. Malek, R. Sooknanan and P. Lens, *J. Virol. Methods*, 1991, **35**, 273–286.
8 P. Lizardi, X. Huang, Z. Zhu, P. Bray-Ward, D. Thomas and D. Ward, *Nat. Genet.*, 1998, **19**, 225–232.
9 M. Nilsson, M. Gullberg, F. Dahl, K. Szuhai and A. K. Raap, *Nucleic Acids Res.*, 2002, **30**, e66.
10 D. Y. Zhang, M. Brandwein, T. Hsuih and H. B. Li, *Mol. Diagn.*, 2001, **6**, 141–150.
11 L. An, W. Tang, T. A. Ranalli, H.-J. Kim, J. Wytiaz and H. Kong, *J. Biol. Chem.*, 2005, **280**, 28952–28958.
12 J. Goldmeyer, H. Kong and W. J. Tang, *J. Mol. Diagn.*, 2007, **9**, 639–644.
13 J. Goldmeyer, H. Li, M. McCormac, S. Cook, C. Stratton, B. Lemieux, H. Kong, W. Tang and Y.-W. Tang, *J. Clin. Microbiol.*, 2008, **46**, 1534–1536.
14 M. Vincent, Y. Xu and H. Kong, *EMBO Rep.*, 2004, **5**, 795–800.
15 Y. Tong, W. Tang, H.-J. Kim, X. Pan, T. A. Ranalli and H. Kong, *BioTechniques*, 2008, **45**, 543–557.
16 T. Notomi, H. Okayama, H. Masubuchi, T. Yonekawa, K. Watanabe, N. Amino and T. Hase, *Nucleic Acids Res.*, 2000, **28**, e63.
17 K. Nagamine, K. Watanabe, K. Ohtsuka, T. Hase and T. Notomi, *Clin. Chem.*, 2001, **47**, 1742–1743.
18 Y. Mori, K. Nagamine, N. Tomita and T. Notomi, *Biochem. Biophys. Res. Commun.*, 2001, **289**, 150–154.
19 E. Aryan, M. Makvandi, A. Farajzadeh, K. Huygen, P. Bifani, S. L. Mousavi, A. Fateh, A. Jelodar, M. M. Gouya and M. Romano, *Microbiol. Res.*, 2010, **165**, 211–220.
20 X. Fang, Y. Liu, J. Kong and X. Jiang, *Anal. Chem.*, 2010, **82**, 3002–3006.
21 X. Fang, H. Chen, S. Yu, X. Jiang and J. Kong, *Anal. Chem.*, 2011, **83**, 690–695.
22 P. Gill, A.-H. Alvandi, H. Abdul-Tehrani and M. Sadeghizadeh, *Diagn. Microbiol. Infect. Dis.*, 2008, **62**, 119–124.
23 A. Motré, R. Kong and Y. Li, *J. Microbiol. Methods*, 2011, **84**, 343–345.
24 W. H. Chow, C. McCloskey, Y. Tong, L. Hu, Q. You, C. P. Kelly, H. Kong, Y. W. Tang and W. Tang, *J. Mol. Diagn.*, 2008, **10**, 452–458.
25 N. Ramalingam, T. San, T. Kai, M. Mak and H.-Q. Gong, *Microfluid. Nanofluid.*, 2009, **7**, 325–336.
26 M. Mahalanabis, J. Do, H. Muayad, J. Y. Zhang and C. M. Klapperich, *Biomed. Microdevices*, 2010, **12**, 353–359.
27 C. Lui, N. C. Cady and C. A. Batt, *Sensors*, 2009, **9**, 3713–3744.
28 B. S. Ferguson, S. F. Buchsbaum, J. S. Swensen, K. Hsieh, X. Lou and H. T. Soh, *Anal. Chem.*, 2009, **81**, 6503–6508.
29 S. S. W. Yeung, T. M. H. Lee and I.-M. Hsing, *Anal. Chem.*, 2008, **80**, 363–368.
30 R. H. Liu, J. Yang, R. Lenigk, J. Bonnano and P. Grodzinski, *Anal. Chem.*, 2004, **76**, 1824–1831.
31 J. S. Swensen, Y. Xiao, B. S. Ferguson, A. A. Lubin, R. Y. Lai, A. J. Heeger, K. W. Plaxco and H. T. Soh, *J. Am. Chem. Soc.*, 2009, **131**, 4262–4266.
32 S. S. W. Yeung, T. M. H. Lee and I.-M. Hsing, *J. Am. Chem. Soc.*, 2006, **128**, 13374–13375.
33 N. Nakamura, K. Ito, M. Takahashi, K. Hashimoto, M. Kawamoto, M. Yamanaka, A. Taniguchi, N. Kamatani and N. Gemma, *Anal. Chem.*, 2007, **79**, 9484–9493.
34 T. Deféver, M. Druet, M. Rochelet-Dequaire, M. Joannes, C. Grossiord, B. Limoges and D. Marchal, *J. Am. Chem. Soc.*, 2009, **131**, 11433–11441.
35 T. Deféver, M. Druet, D. Evrard, D. Marchal and B. Limoges, *Anal. Chem.*, 2011, **83**, 1815–1821.
36 K. Maruyama, Y. Mishima, K. Minagawa and J. Motonaka, *J. Electroanal. Chem.*, 2001, **510**, 96–102.
37 Z. Wang, A. Sekulovic, J. P. Kutter, D. D. Bang and A. Wolff, *Electrophoresis*, 2006, **27**, 5051–5058.
38 D. L. House, C. H. Chon, C. B. Creech, E. P. Skaar and D. Li, *J. Biotechnol.*, 2010, **146**, 93–99.